

## Atmospheric pressure argon surface discharges propagated in long tubes: physical characterization and application to bio-decontamination

This content has been downloaded from IOPscience. Please scroll down to see the full text.

2015 J. Phys. D: Appl. Phys. 48 464003

(<http://iopscience.iop.org/0022-3727/48/46/464003>)

View [the table of contents for this issue](#), or go to the [journal homepage](#) for more

Download details:

IP Address: 128.141.184.127

This content was downloaded on 15/10/2015 at 16:36

Please note that [terms and conditions apply](#).

# Atmospheric pressure argon surface discharges propagated in long tubes: physical characterization and application to bio-decontamination

Zuzana Kovalova<sup>1,2</sup>, Magali Leroy<sup>1</sup>, Carolyn Jacobs<sup>1</sup>,  
Michael J Kirkpatrick<sup>1</sup>, Zdenko Machala<sup>2</sup>, Filipa Lopes<sup>3</sup>,  
Christophe O Laux<sup>4</sup>, Michael S DuBow<sup>5</sup> and Emmanuel Odic<sup>1</sup>

<sup>1</sup> GeePs—Group of electrical engineering—Paris UMR CNRS 8507, CentraleSupélec, Univ Paris-Sud, Sorbonne Universités, UPMC Univ Paris 06 91192 Gif-sur-Yvette, France

<sup>2</sup> Faculty of Mathematics, Physics and Informatics, Comenius University in Bratislava, 84248 Bratislava, Slovakia

<sup>3</sup> Laboratoire de Génie des Procédés et Matériaux LGPM, CentraleSupélec, 92295 Châtenay-Malabry, France

<sup>4</sup> Laboratoire d'Énergétique Moléculaire et Macroscopique, Combustion EM2C, CNRS UPR 288, CentraleSupélec, 92295 Châtenay-Malabry, France

<sup>5</sup> Laboratoire de Génomique et Biodiversité Microbienne des Biofilms, Institute for Integrative Biology of the Cell (I2BC), CEA, CNRS, Université Paris-Saclay, Université Paris-Sud, Bâtiment 409, 91405 Orsay, France

E-mail: [emmanuel.odic@centralesupelec.fr](mailto:emmanuel.odic@centralesupelec.fr)

Received 26 June 2015, revised 6 August 2015

Accepted for publication 13 August 2015

Published 15 October 2015



## Abstract

Pulsed corona discharges propagated in argon (or in argon with added water vapor) at atmospheric pressure on the interior surface of a 49 cm long quartz tube were investigated for the application of surface bio-decontamination. H<sub>2</sub>O molecule dissociation in the argon plasma generated reactive species (i.e. OH in ground and excited states) and UV emission, which both directly affected bacterial cells. In order to facilitate the evaluation of the contribution of UV radiation, a DNA damage repair defective bacterial strain, *Escherichia coli* DH-1, was used. Discharge characteristics, including propagation velocity and plasma temperature, were measured. Up to ~5.5 and ~5 log<sub>10</sub> reductions were observed for *E. coli* DH-1 bacteria (from 10<sup>6</sup> initial load) exposed 2 cm and 44 cm away from the charged electrode, respectively, for a 20 min plasma treatment. The factors contributing to the observed bactericidal effect include desiccation, reactive oxygen species (OH) plus H<sub>2</sub>O<sub>2</sub> accumulation in the liquid phase, and UV-B (and possibly VUV) emission in dry argon. The steady state temperature measured on the quartz tube wall did not exceed 29 °C; the contribution of heating, along with that of H<sub>2</sub>O<sub>2</sub> accumulation, was estimated to be low. The effect of UV-B emission alone or in combination with the other stress factors of the plasma process was examined for different operating conditions.

Keywords: bio-decontamination, low-temperature plasma, *Escherichia coli* DH-1, atmospheric pressure argon pulsed corona discharge, UV emission, long dielectric tube

(Some figures may appear in colour only in the online journal)

## 1. Introduction

According to Bryers [1], nosocomial infections are the fourth leading cause of death in the U.S., with over 2 million cases per year. Most cross-contamination results from an insufficient surface sterilization of medically invasive tools, in particular of thermally sensitive materials that cannot withstand wet heat treatment, i.e. autoclaving. Alternate surface sterilization techniques are therefore necessary. Over the course of the last decade, non-thermal plasma technologies have been investigated for medical purposes and surface decontamination [2, 3] using different plasma sources and operating pressures. Both early [4–6] and more recent works [7, 8] have been conducted in reduced pressure conditions, but the current trend is to work at atmospheric pressure [3, 9–13], mainly due to operational constraints and the demand for medical applications. In the field of surface sterilization of thermally sensitive materials, the decontamination of small diameter tubes (e.g. catheters, endoscopes) is an important issue. The exposure mode of the surface was also considered. In previous studies, the inner surfaces of tubes were exposed to different plasma processes at atmospheric pressure in direct [14] or remote exposure modes. For the remote exposure mode, a flowing post-discharge was passed through the tube inlet. The plasma source was either a pure nitrogen corona discharge producing an emissive afterglow [15], or a humid argon dielectric barrier discharge [16]. In the latter case, argon was preferred to air as a feed gas in order to avoid the formation of ozone and nitrogen oxides (and nitric acid if water is present [17, 18]) that may damage the treated surface. Furthermore, water dissociation in an argon discharge is much more efficient than in air or nitrogen [19].

The overall objective in the presented work is the decontamination of small diameter long tubes by direct exposure of the tube inner surface to the discharge plasma. Pulsed corona discharges were propagated on the inner walls of dielectric tubes with the argon flow at atmospheric pressure. The discharge was first characterized in terms of propagation length and velocity, relative emission intensity, and thermal behavior. Bactericidal tests were conducted for increasing exposure time with regard to sample location in the tube. An effort was made to quantify the contribution of the different factors to the overall bactericidal effect, with a particular emphasis on the contribution of UV emissions. Toward this objective, we studied the bactericidal effects of the argon plasma in this system on bacteria placed inside a quartz tube—directly exposed to the plasma (including UV light), versus bacteria placed on the outside surface of the tube—only exposed to UV emission. To facilitate the study, we used the *recA-E. coli* strain DH-1 in order to obtain a large mortality response to UV light exposure.

## 2. Materials and methods

### 2.1. Plasma device, high voltage power supply, and electrical measurements

So-called plasma bullets produced by pulsed dielectric barrier discharges propagating with very high velocities in dielectric

capillaries were previously obtained and studied with neon, helium or argon as feed gas [20–24]. In the present study, the discharge device is quite similar to a Single Electrode Jet [25], but with a counter electrode at the tube outlet (figure 1). Pulsed corona discharges were propagated on the inner surfaces of a quartz tube (8 mm inner diameter, variable length: 49 cm in the case of figure 1), in which argon (3.9 slm in dry argon conditions and 4.7 slm in a 760 ppm water vapor/argon mixture) was flowing at atmospheric pressure, from a tungsten needle placed at the tube inlet to a grounded counter electrode located at its outlet. The tungsten needle was connected to a low jitter, pulsed high voltage power supply made from a MOSFET solid switch bridge (Behlke HTS 301) with a 2 nF charging capacitor fed by a dc 30 kV–10 mA high voltage power source. Positive voltage pulses of up to 35 kV peak value (due to the inductance of the circuit) and 200 ns–5  $\mu$ s width were obtained with a repetition rate of 500 pulses  $s^{-1}$ . The voltage pulse rise time was  $\sim 1$  kV  $ns^{-1}$ . A voltage probe (Tektronix P6015A, 1 V: 1000 V–75 MHz) connected to the needle electrode and a fast rise current transformer (Tektronix CT-2, 1 mV: 1 mA–200 MHz) connected to the counter electrode were used for voltage and current measurements, respectively. Signals were recorded using a LeCroy WaveRunner 62 Xi digital oscilloscope (600 MHz–10 GS  $s^{-1}$ ).

### 2.2. Optical emission spectroscopy

Optical emission relative intensity and plasma rotational temperature were measured by optical emission spectroscopy (OES) along the quartz tube. OES was performed in the 250–850 nm range using an Acton Standard Series SP-2758 imaging spectrograph of focal length 750 mm. Two gratings were used in the measurements; a 2400  $gr\ mm^{-1}$  ruled grating blazed at 240 nm and a 300  $gr\ mm^{-1}$  ruled grating blazed at 300 nm. This spectrograph was coupled to a Princeton Instruments PI-MAX4:1024f-RB intensified CCD camera with 1024  $\times$  1024 pixels. The pixel size was 13  $\times$  13  $\mu$ m. For the 2400 lines  $mm^{-1}$  grating, the spectral resolution of the system was found to be 0.025 nm (full-width-at-half-maximum).

For all spectroscopic measurements, light was collected by fiber optic cable pointed perpendicularly at the tube from a distance of 38 cm. This fiber was moved along the tube's length in order to collect light from different positions. A collimator was added to the fiber optic cable and adjusted to collect light from a 1 cm diameter disk centered on the tube axis.

For spectroscopic measurements used for the evaluation of the transient plasma temperature, the light was collected at each position along the tube by taking the average of 1000 exposures, each consisting of 100 on-CCD accumulations of 600 ns duration.

For time-resolved measurements, the light was collected for durations of 10 ns; 300 of these 10 ns spectra were taken during and after the 2  $\mu$ s duration voltage pulse. Each of these 300 spectra was obtained using the average of 3 exposures consisting of 100 on-CCD accumulations.

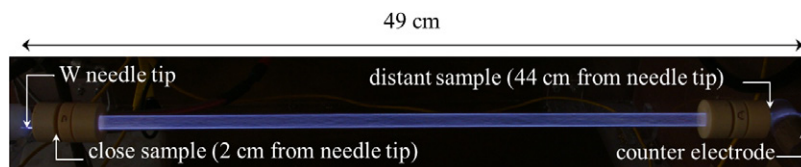


**Figure 1.** Photograph of the pulsed corona discharge propagating in argon gas inside an 8 mm inner diameter quartz tube over 49 cm between a charged tungsten needle and a grounded counter electrode. The bacterial sample locations at 2 and 44 cm are indicated.

### 2.3. Temperature measurements

Local rotational temperature measurements were performed during the discharge propagation. At atmospheric pressure, it is assumed that the rotational temperature is equal to the kinetic (gas) temperature [26]. Thus, 1000 ppm of nitrogen was added to the gas mixture in order to evaluate the neutral gas temperature in the plasma. The spectral emission of the  $N_2$  second positive system between 377 and 381 nm (0–2 band) was measured at various locations (2.5, 5, 15, 25, and 40 cm from the needle electrode) along the tube. Comparisons between the measured spectra and spectra calculated using the line-by-line radiation code SPECAIR [27] were used to estimate the rotational temperature of the plasma.

Under steady-state operating conditions, the bulk gas temperature at the tube outlet and the quartz tube outer surface temperature were measured using an alcohol thermometer. The bulk gas temperature was measured in the flow and behind the counter electrode at 51 cm from the source electrode (i.e. 3 cm downstream of the discharge region). The external surface temperature of the quartz tube was measured at two locations: 2 and 44 cm from the needle electrode. In this case, the thermometer was sealed in a 2 cm thick Plexiglas casing and its tip coated with a heat transfer silicon paste (HTSP—Electrolube) that was directly applied to the outer quartz surface.

### 2.4. Bacterial sample and test conditions

**Bacterial strains and culture conditions.** *E. coli* strain DH-1 (F<sup>-</sup>,  $\lambda^-$ , *endA1*, *recA1*, *gyrA96*, *thi-1*, *glnV44*, *relA1*, *hsdR17*) was used for all experiments. We have chosen such a UV sensitive (*recA*<sup>-</sup>) *E. coli* strain [28] in order to obtain a large mortality response to UV light exposure. Bacteria were cultured in Miller's modified Luria broth LB medium (CONDA) at 37 °C with agitation until stationary phase, then frozen with 20% (v/v) glycerol in 20  $\mu$ l aliquots titered at  $\sim 10^9$  colony forming units (CFU)/ml.

### 2.5. Plasma treatment bactericidal assay

Aliquots of bacterial cultures were thawed and resuspended in 110  $\mu$ l 1/3X LB. Droplets of 10  $\mu$ l volume were placed inside or outside the quartz tube (in order to evaluate the UV-B effect on bacteria viability—see section 3.4), and either immediately treated as droplets (liquid) or dried at room temperature (2–4 h) or under argon flow (10 min) before treatment. Samples were positioned at 2 and 44 cm from the needle electrode (figure 1) and simultaneously exposed to plasma treatment at room temperature for up to 20 min. Samples exposed for the same duration to the argon flow alone were also included as controls.

Bacterial cells were recovered with 10 repetitive rinsings of the inner or outer quartz tube surface with a total of 100  $\mu$ l sterile distilled water and immediately resuspended in 1/3X LB. Recovered samples were serially diluted or concentrated by filtration through a 0.45  $\mu$ m mixed cellulose ester membrane (Millipore) when high mortality was expected, plated on LB agar, incubated at 37 °C overnight, and quantified by colony counting. Samples and controls were exposed to either 3.9 slm (1.3 m s<sup>-1</sup> average velocity) dry argon, or 4.7 slm (1.55 m s<sup>-1</sup>) humid argon (760 ppm H<sub>2</sub>O) with an initial 2 min gas purge. Assays were carried out in triplicates (unless otherwise specified).

### 2.6. H<sub>2</sub>O<sub>2</sub> assay

Hydrogen peroxide accumulation in water droplets inside the quartz tube was measured by optical absorption spectroscopy, as H<sub>2</sub>O<sub>2</sub> reacts with ammonium vanadate in an acidic environment (dipicolinic acid, distilled water, sulfuric acid) to form a yellow complex with a maximum absorption at 430 nm [19]. A linear relation,  $[H_2O_2]_{mg/l} = Abs_{432\text{ nm}} \times 704$ , was obtained between the absorbance of the complex and the hydrogen peroxide concentration for H<sub>2</sub>O<sub>2</sub> solution concentrations ranging from 0 to 300 mg l<sup>-1</sup>. Five droplets of 10  $\mu$ l distilled water (50  $\mu$ l total) were deposited in the tube at 2 and 44 cm from the source electrode. After exposure to the discharge in humid argon (760 ppm H<sub>2</sub>O, 4.7 slm) for 1 to 5 min, the droplets were collected all together in one volume (50  $\mu$ l) from the quartz tube and diluted 1/10 in the reagent solution. The bactericidal effect of the measured H<sub>2</sub>O<sub>2</sub> concentrations was evaluated by control experiment: incubating 10  $\mu$ l of bacterial culture aliquots, prepared the same way as for the plasma treatment, for 5 min in final concentrations of 53 to 222 mg l<sup>-1</sup> H<sub>2</sub>O<sub>2</sub>. Samples were handled with the same protocol used following the plasma treatment. Briefly, samples were immediately diluted in 100  $\mu$ l sterile distilled water and mixed in 900  $\mu$ l 1/3 LB before being serially diluted and plated for viable titer determination.

## 3. Results

### 3.1. Choice of the discharge operating conditions

Typical voltage and current waveforms are presented in figure 2 for two different distances between the needle electrode (tube inlet) and the counter electrode (tube outlet). The current pulse, corresponding to the arrival of the propagating discharge at the counter electrode, is delayed from the voltage front rise (from which the discharge is initiated). For a given

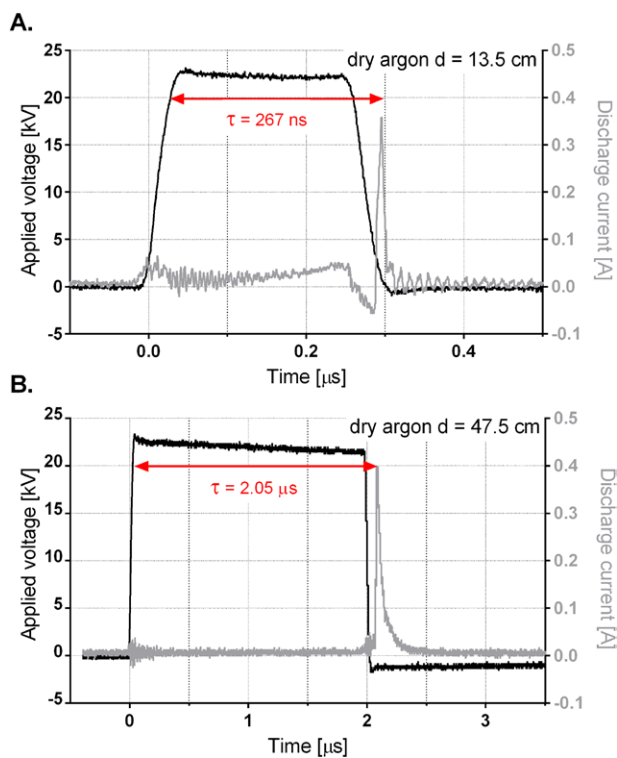


**Figure 2.** Voltage and current waveforms for two needle-to-counter-electrode gap distances for a discharge in dry argon gas (3.9 slm). (A) Gap distance of 13.5 cm, and (B) gap distance of 47.5 cm, with  $\tau$  being the delay from the voltage pulse rise to the arrival of the propagating discharge to the counter electrode.

constant peak voltage value, this delay  $\tau$  is associated with discharge propagation velocity and therefore,  $\tau$  depends on the gap (tube) length  $d$ . For given values of the peak voltage and the gap length, the pulse width was adjusted in order to avoid a spark discharge, while ensuring that the discharge propagated along the full length of the tube. This situation corresponds to an optimum pulse width, for which the current pulse is obtained during or immediately after the voltage drop (figure 2). In physical terms, the filamentary discharge tip just reached the counter electrode when the applied voltage approached 0.

The discharge propagation length, i.e. full propagation of the discharge from the needle electrode to the counter electrode, was investigated as a function of both the voltage pulse peak value and width. For a fixed pulse width (700 ns for figure 3(A)) and a constant 550 mA current pulse amplitude (occurring after the voltage drop), the propagation length increased linearly with the peak voltage. The slope of this curve can be identified as the mean electric field in the discharge channel, also referred to as the stability field. Values of  $520 \text{ V cm}^{-1}$  and  $590 \text{ V cm}^{-1}$  were obtained in dry and humid argon (760 ppm  $\text{H}_2\text{O}$ ), respectively. In dry air at atmospheric pressure, this value is  $5 \text{ kV cm}^{-1}$ , whereas  $400 \text{ V cm}^{-1}$  was found for an atmospheric pressure argon volume discharge [29]. The higher value of the stability field calculated in humid conditions is attributed to electron energy losses in dissociative, vibrational, and rotational mechanisms with water, leading to a higher applied voltage for a given propagation

length. For a fixed peak voltage value (23.3 kV for figure 3(B)) and a constant 450 mA current pulse amplitude (occurring after the voltage drop), the propagation length increases with pulse width, until it reaches a saturation point  $2.5 \mu\text{s}$  beyond which increasing the pulse duration no longer increased the propagation length. Such results were previously observed for the length of plasma jet (helium plasma jet propagated in open air [24]).

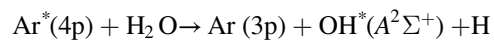
By measuring voltage and current waveforms as presented in figure 2, it was possible to estimate the average discharge velocity using the ratio  $d/\tau$ . Average velocities of  $5 \times 10^5 \text{ ms}^{-1}$  and  $2.3 \times 10^5 \text{ ms}^{-1}$  were calculated for short (13.5 cm) and long (47.5 cm) gaps, respectively (figure 2). These values are consistent with those measured optically in a comparable situation - streamers propagating in argon over a dielectric surface [30].

The water vapor concentration for which the discharge could be fully propagated along the tube with a peak voltage value lower than 30 kV was found to be 760 ppm. The above mentioned measurements led to the final settings for electrical parameters according to the propagation length. For all bactericidal tests, the plasma was generated with a 2–2.2  $\mu\text{s}$  voltage pulse at 500 pulses  $\text{s}^{-1}$  with a 20.6–27.9 kV peak voltage depending on the sample and the gas humidity.

It is worth mentioning that by using the same electrode arrangement and high voltage power supply, the propagation length of more than one meter was obtained in a thin (2 mm inner diameter) silicone tube with pure argon flowing at atmospheric pressure. This result has important medical implications since the plasma source device under investigation could possibly be applied to catheter and endoscope duct decontamination. However, for the research reported here, aimed at the decontamination mechanism investigation, the shorter quartz tube device described above was preferred.

### 3.2. Plasma optical emission

Optical emission spectra of the pulsed corona discharge plasma in dry and humid argon (figure 4) showed the presence of emissive OH radicals. In the presence of water (even traces, as it is for 'dry' Ar condition), the argon plasma generates ultraviolet (UV-B) emission through the de-excitation of  $\text{OH}^*$  [ $A^2\Sigma^+ - X^2\Pi$ ] radicals (305–311 nm), themselves mainly produced by a water dissociation mechanism involving  $\text{Ar}^*$ :



As expected, the relative intensity of the OH band depends on the humidity present in the feed gas and it is greater in argon with 760 ppm of water vapor than in dry argon [31]. In our conditions, 760 ppm was the water vapor concentration for which the discharge could be fully propagated along the tube with a peak voltage value lower than 30 kV. This water vapor concentration is slightly below the optimum value, above which increasing the water vapor content does not lead to an increase in the OH line intensity, but on the contrary leads to its decrease. This result was previously observed and was found to be caused by quenching mechanisms that become

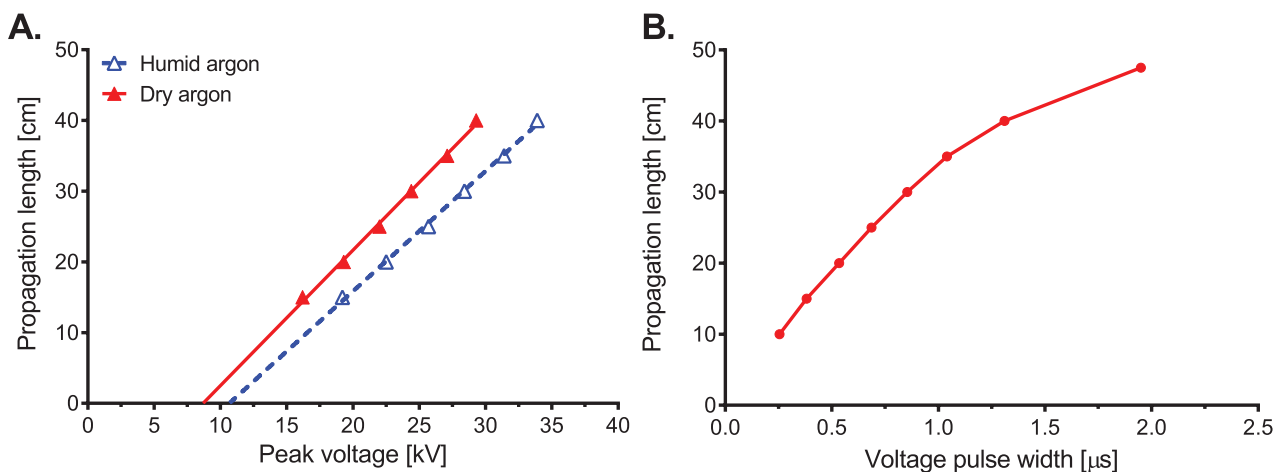


**Figure 3.** Pulsed corona discharge electrical characterization. (A) Discharge propagation length at constant pulse width (700 ns) for increasing peak voltage in humid argon (4.7 slm, blue symbols), and dry argon (3.9 slm, red symbols) with linear fits (dashed lines). (B) Discharge propagation length at constant peak voltage (23.3 kV) for increasing pulse width in dry argon.

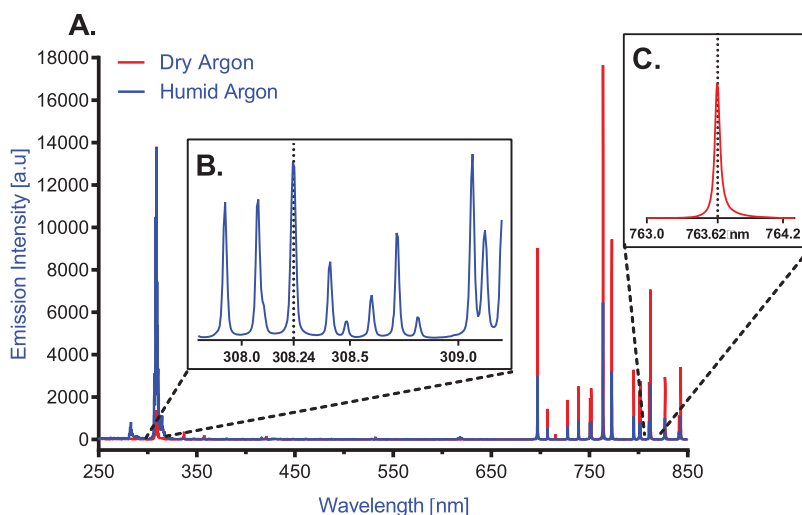
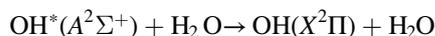


**Figure 4.** (A) Optical emission spectra of the pulsed corona discharge in dry (red line) and humid argon (blue line) acquired at 5 cm from the HV electrode. Detector integration time 600 ns, grating 300 lines  $\text{mm}^{-1}$ . (B) Spectrum of the rotational bands of OH [ $A^2\Sigma^+ - X^2\Pi$ ] measured in humid argon (760 ppm water vapor), grating 2400 lines  $\text{mm}^{-1}$ . (C) Ar emission line in dry argon, grating 1800 lines  $\text{mm}^{-1}$ .

the dominant phenomena in high water vapor concentration conditions [31, 32] as per:



The presence of humidity in the feed gas has thus a dual benefit of producing both reactive OH radicals and UV-B emission.

The time-resolved and spatial distribution of the OH radical emission intensity along the length of the quartz tube was measured by recording the optical emission centered at 308 nm (305–311 nm range). Figure 5 shows the evolution of OH emission intensity profile with time (the time delay from a command pulse rise) for 9 different light collecting positions along the tube. The time delay of the OH emission maxima with respect to the voltage front rise increases with the enlarging distance between the high voltage electrode and the light collecting position, so confirming a streamer type propagation mechanism, and allows for calculation of the instantaneous propagation velocity (figure 6). The obtained values are again in good agreement with the average velocity values

previously calculated using the electrical measurements and with velocity values from literature with argon gas [30], and helium gas [33, 34]. The values of propagation velocity obtained here in humid argon are lower than those obtained in dry argon conditions. As an example, at fixed applied voltage (26.5 kV), the average propagation velocity was reduced by 8% for a 10 cm propagation length and up to 30% for a 35 cm propagation length when discharge feed gas was changed from dry argon to humid. This is attributed to electron energy losses in dissociative, vibrational, rotational and attachment mechanisms with water.

Another interesting feature is that for each measurement location, the second emission maximum occurs just after the applied voltage drop (at 2.4  $\mu\text{s}$ ), suggesting a back discharge mechanism. This second emission peak also exhibits propagation mechanisms, but with higher velocity (4 to 6 times higher), and it accounts for a significant part of the overall emission intensity per propagation event: from 40 to 50% of the integrated relative intensity according to the location (this

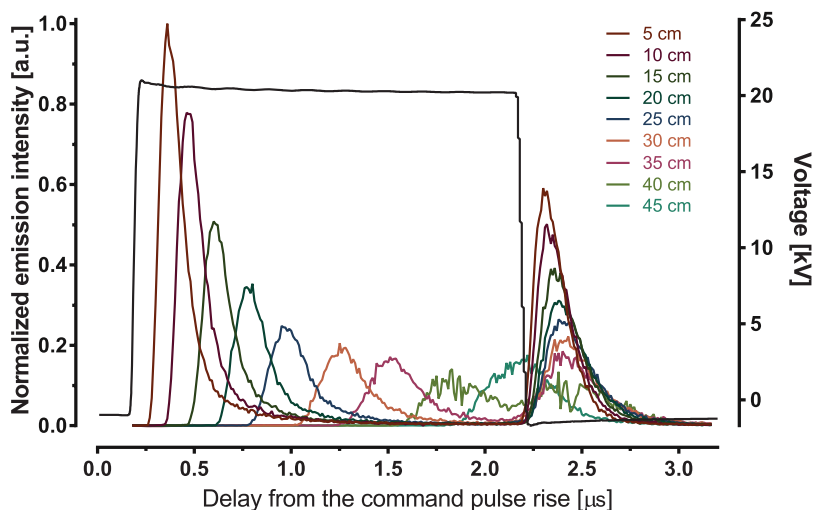


**Figure 5.** Excited  $\text{OH}^*$  [ $A^2\Sigma^+-X^2\Pi$ ] radicals emission (305–311 nm) relative intensity profile evolution with time for different light collecting positions along the tube (distance from the needle electrode: 5, 10, 15, 20, 25, 30, 35, 40, 45 cm) and synchronized applied voltage signal. Humid argon (760 ppm  $\text{H}_2\text{O}$ , 4.7 slm).

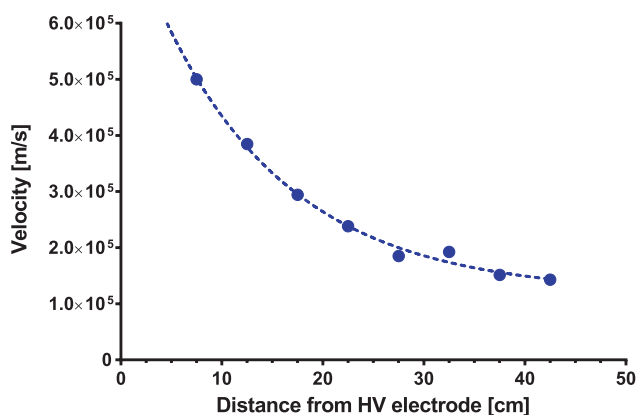


**Figure 6.** Discharge instantaneous velocity of propagation in argon with water vapor (calculated from a fit of the data of figure 5).

interesting phenomenon will not be discussed in this paper). This integrated relative intensity per discharge event corresponds to a relative dose per discharge event which exponentially decreased with increasing distance from the HV needle electrode (figure 7). According to this exponential decrease of the emission with the distance, the bacteria sample located at 2 cm is exposed to a dose 4.2 times higher than the bacteria sample located at 44 cm from the HV electrode.

### 3.3. Temperature

Measurements of the gas temperature are required because any considerable increase of the temperature can play an important biocidal role.

Therefore, the rotational temperature in the discharge channel was measured by emission spectroscopy of the 2nd positive  $\text{N}_2$  system, and found to be  $450 \pm 50$  K for both dry and humid argon gas conditions at all measurement locations between 2.5 and 40 cm from the needle electrode (figure 8). This rotational (i.e. gas) temperature was a maximum value

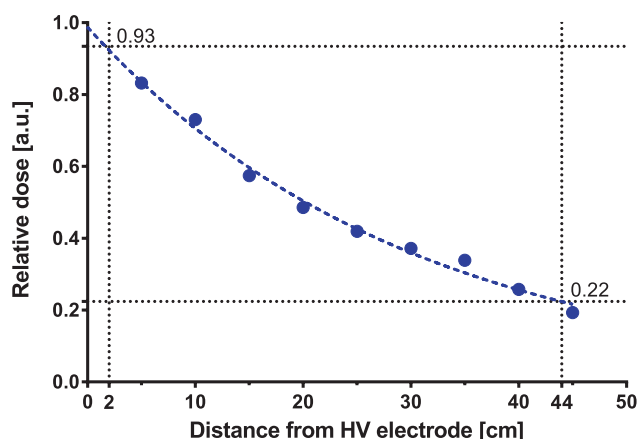


**Figure 7.** Relative UV-B dose (305–311 nm) per discharge event calculated for each position from the data of figure 5, including the second emission maximum at 2.4  $\mu\text{s}$ .

measured over a 600 ns time interval for a discharge phenomenon with overall durations of 2–2.2  $\mu\text{s}$  and a 500 pulses  $\text{s}^{-1}$  repetition rate.

We also measured the mean gas temperature increase in the bulk gas phase (at the tube outlet) and on the outer surface of the quartz tube at 2 and 44 cm from the HV electrode in both dry and humid argon. A maximum temperature elevation of 2.2  $^\circ\text{C}$  (figure 9(A)) was recorded for the post-discharge argon flow (at the counter electrode), while a maximum increase of 4.0  $^\circ\text{C}$  (figure 9(B)) was measured on the external tube surface at 2 cm after 20 min of discharge operation in humid argon. The presence of water traces in the argon gas required a higher applied voltage to propagate the discharge over the same distance and resulted in a higher measured temperature at the quartz surface. The increase of the surface temperature during the plasma treatment was smaller at higher distances from the source electrode. As the plasma process was carried out at room temperature (25  $^\circ\text{C}$ ), the measured temperature always remained below 30  $^\circ\text{C}$ .

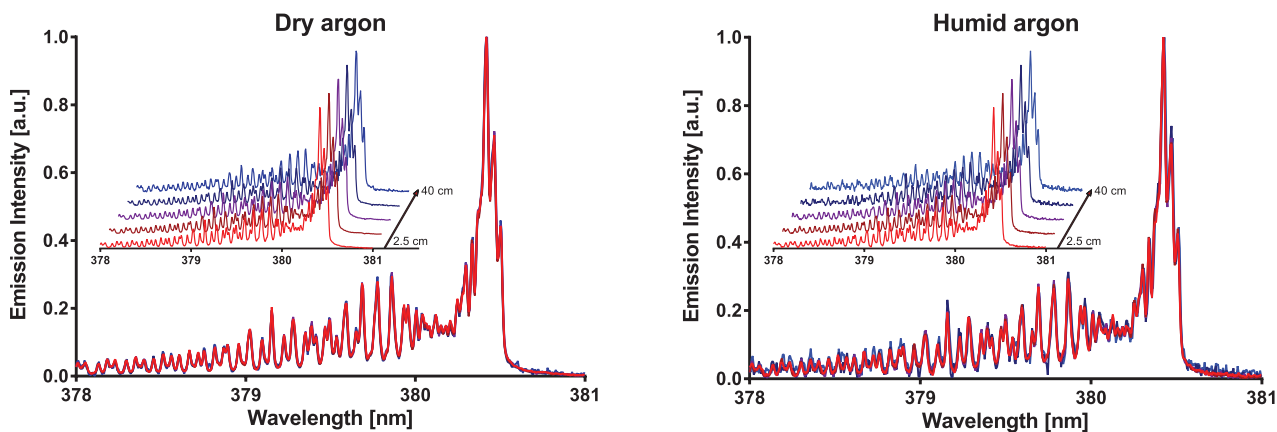


**Figure 8.** Optical emission spectra of the N<sub>2</sub> second positive system between 378 and 381 nm (0–2 band) measured at various locations (2.5, 5, 15, 25, and 40 cm from the needle electrode, overlaid) along the quartz tube (A) in dry argon and (B) humid argon (760 ppm H<sub>2</sub>O). Small graphs show spectra from all five locations.

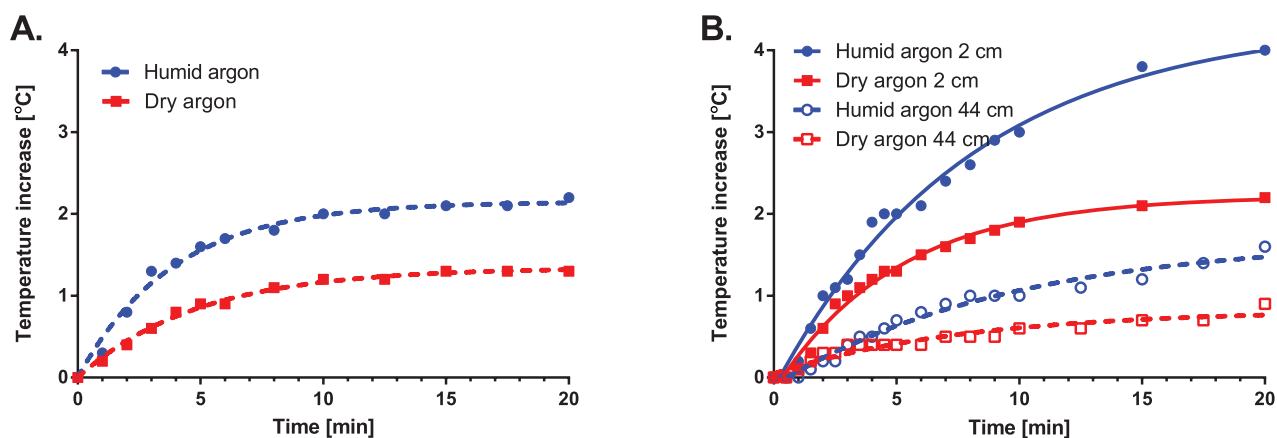


**Figure 9.** Absolute temperature increase over treatment times of (A) the feed gas measured at the counter electrode in dry (red) and humid argon (blue), and (B) quartz tube surface at 2 (circle symbols) and 44 cm (square symbols) from the source electrode (needle), with one phase exponential fits (lines).

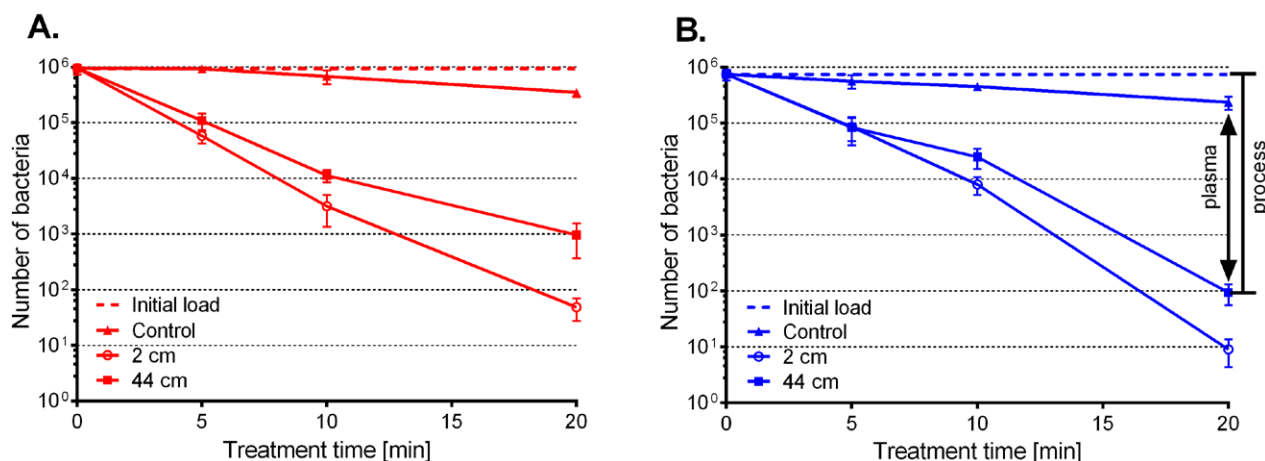


**Figure 10.** Bacterial viability reduction over increasing treatment times in (A) dry argon (red) and (B) humid argon feed gas (blue). No sample drying prior to treatment (liquid samples). Viable bacterial cells (colony forming units) recovered after 0 (initial bacterial load, dashed line) 5, 10, and 20 min of exposure to argon flow only (controls: triangle symbols for both locations) and argon plasma at 2 (circle symbols) and 44 cm (square symbols) from the source electrode. Assays were carried out in triplicates. Graphed: mean  $\pm$  SEM.

### 3.4. Bactericidal effect

We investigated the decontamination efficiency of the pulsed corona atmospheric pressure argon plasma at the inner

surfaces of the quartz tube. Starting from a population of  $\sim 10^6$  cultivable *E. coli* DH-1 cells, we evaluated the bactericidal effect of the plasma for samples placed inside the tube for two

locations, 2 cm and 44 cm from the HV needle electrode. The survival curves of bacteria in argon (A) or argon with 760 ppm water vapor (B) plasma are presented in figure 10. Although dry or humid (760 ppm water vapor) argon may cause desiccation, our control measurements showed they had no significant effect on bacterial survival in our experiments (two-tailed Wilcoxon matched-pairs signed rank test;  $p$  value = 0.25).

The plasma in dry argon reduced the bacterial population by up to 4  $\log_{10}$  after a 20 min exposure for the sample located 2 cm from the needle electrode. For the sample at 44 cm distance, the reduction in viability was 2.5  $\log_{10}$  after 20 min. Two intermediate time points were also measured, with smaller differences between the 2 and 44 cm samples: a 5 min exposure reduced the bacterial population by 1 and 1.2  $\log_{10}$  and a 10 min exposure by 2 and 2.5  $\log_{10}$ , for the 44 and 2 cm bacterial samples, respectively.

In the humid argon plasmas, a 0.95  $\log_{10}$  reduction in bacteria viability was observed after a 5 min exposure for both sample locations. After a 10 min exposure, we obtained reductions of 1.5 and 2  $\log_{10}$  for 44 and 2 cm bacterial samples, respectively. Up to 5  $\log_{10}$  reduction was reached after a 20 min exposure for the sample at 2 cm, and 4  $\log_{10}$  for the 44 cm distance.

The decrease in the bactericidal activity over the tube length (figure 10) is likely related to a decrease in the concentration of OH radicals and associated UV-B radiation.

The water content (in argon gas or at the sample level, dried or not) was an important parameter in our experiments since it was shown to be a key parameter that strongly influenced the generation of reactive species by atmospheric-pressure argon plasma jet and its effect on cells [35]. In order to get better understandings of the factors affecting plasma bactericidal effect, several combinations of humid/dry argon gas and liquid/dried bacterial samples were investigated over time (figure 11). The bactericidal effect of the treatment is presented in terms of 'reduction factor', defined as:  $\log_{10}(N_0/N)$  where  $N_0$  is the control sample CFU and  $N$  the sample after plasma treatment CFU. First, let us focus on the samples located inside the tube. As expected, increased treatment times resulted in increased bio-decontamination efficiency. In general, when comparing treatments of liquid versus dried samples, we measured greater decontamination efficiency on dry samples for both positions (2 cm and 44 cm). For example, up to a 5.5 reduction factor ( $\log_{10}$  bacterial reduction) was achieved in the case of humid argon with dry samples 2 cm from needle electrode and 20 min exposure. In the same conditions, a 4.9 reduction factor was obtained at 44 cm. At 20 min exposure time, comparison between humid and dry argon plasma demonstrated greater or equal decontamination efficiency for humid argon. The best decontamination efficiency was obtained in humid argon plasma on dried samples.

Similarly, we measured the bactericidal effect of UV-B plasma radiation alone on liquid and dried samples located outside the quartz tube for argon plasmas produced with both dry and humid feed gas.

As expected from the OES results acquired at different locations along the discharge propagation length (figures 5 and 7), UV-B emission is more intense closer to the HV

electrode and generally has a greater biocidal efficiency at 2 cm than at 44 cm in all conditions tested. The biocidal activity of emission at 308 nm is cumulative, and the decontamination efficiency tends to increase with treatment time in all conditions, reaching a maximum efficiency of 2.35 reduction factor for 20 min treatment of a liquid sample with a humid argon feed gas at 2 cm. The discharge in humid argon with a liquid sample, while not the most efficient when looking at the decontamination efficiency of the overall plasma treatment process (inside tube), generated the best efficiency of decontamination for UV-B radiation alone (outside tube).

### 3.5. Hydrogen peroxide

The impact of  $H_2O_2$  was investigated and its concentration measured in five 10  $\mu$ l water droplets (see section 2.6) exposed to a humid argon discharge as described in Dodet *et al* [19].

Due to evaporation, exposure times greater than 5 min did not allow for the recovery of sufficient liquid volume (10  $\mu$ L), and thus prevented measurements of  $H_2O_2$  accumulation in the liquid phase (figure 12). The reduction of volume through desiccation concentrates  $H_2O_2$  in the liquid phase, resulting in a non-linear concentration with time. As seen in figure 12, with 760 ppm water vapor content,  $H_2O_2$  accumulated faster and in higher concentration near the HV electrode, where the surface temperature was slightly higher (figure 9(B)). For a 5 min exposure time, 222  $mg\ l^{-1}$   $H_2O_2$  was measured at 2 cm and 53  $mg\ l^{-1}$   $H_2O_2$  at 44 cm.

## 4. Discussion

Even if bactericidal, cytotoxic, fragmentation, and denaturation effects have been shown to be stronger in air plasmas such as transient arc than in noble gas plasmas [36], the latter allow propagating the discharge in the insulating tube and prevents the formation of species leading to the degradation of polymers (ozone, nitrogen oxides, nitric acid). The overall objective of this work was to identify various factors accounting for the bactericidal effect of the non-thermal atmospheric pressure argon plasma generated by pulsed corona discharge propagated over long distance on the inner walls of an insulating tube (treatment of the inner walls of long tubes, such as those used for colonoscopy). The biocidal factors generally invoked are UV emission and oxidative chemical species. Damage to DNA may occur through chemical modification (alkylation or oxidation), cross-linking, or base removal such as depurination [37, 38]. The efficiency of the plasma is based on a combination of these factors [39]. Therefore, the bacterial cell death likely results from the accumulation of irreversible oxidative damage to the membrane layers, proteins, and DNA caused by the synergy of the plasma biocidal factors [40–42]. Additional sources of stress generated by the plasma process should be considered, such as damage from desiccation and thermal stresses which could contribute to the overall decontamination effect.

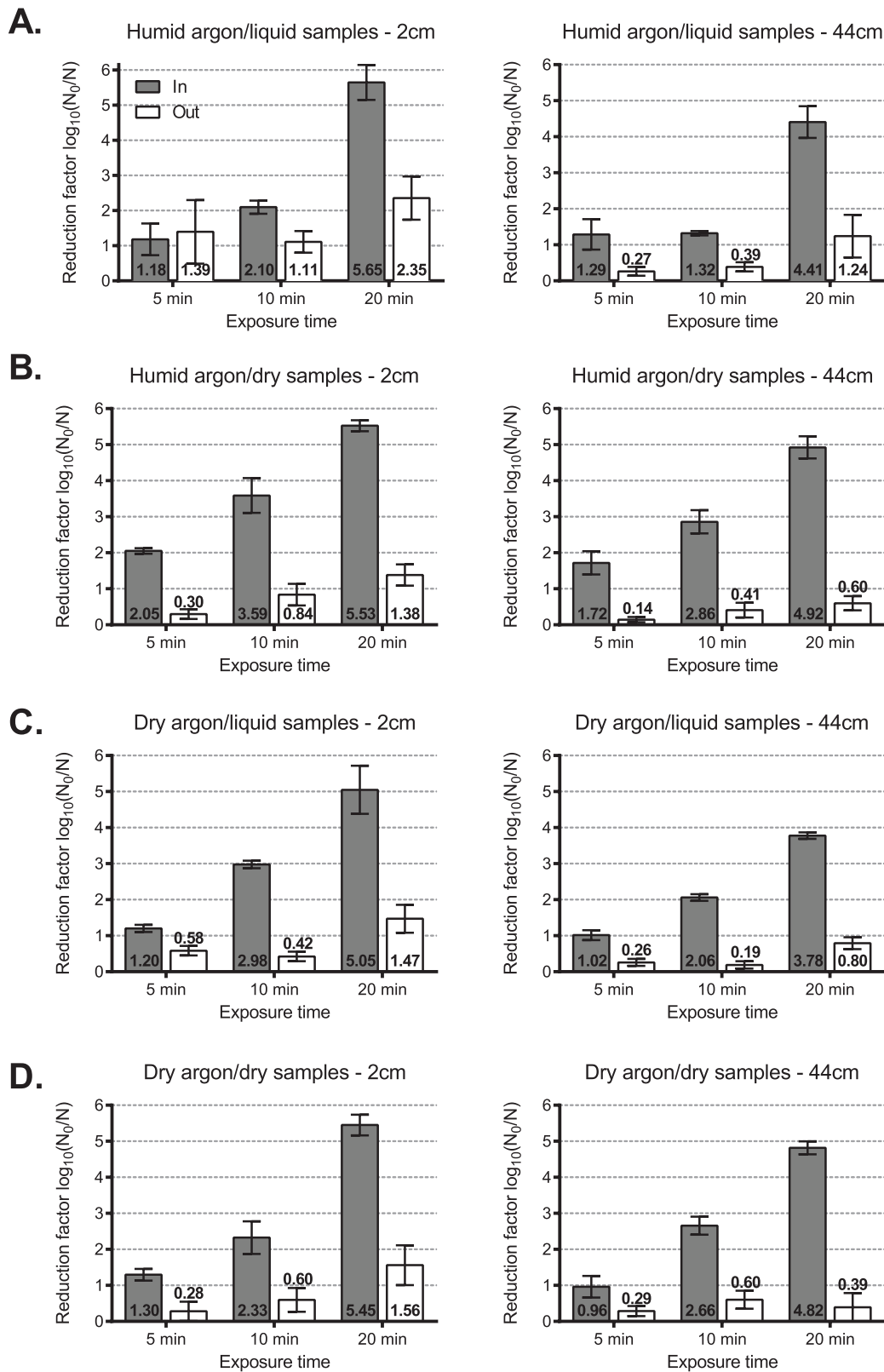


**Figure 11.** Reduction factor measured after the argon plasma treatment (IN, grey bars) and the argon plasma-generated UV-B radiation (OUT, white bars) for increasing exposure times at 2 (left panels) and 44cm (right panels) in various humidity conditions (feed gas and bacterial sample). Reduction factor is calculated as  $\log_{10}(N_0/N)$  where  $N_0$  is the CFU control sample and  $N$  the sample after plasma treatment. Conditions tested were: (A) humid argon & liquid sample, (B) humid argon & dried sample, (C) dry argon & liquid sample, and (D) dry argon & dried sample. Assays were carried out in triplicates (except for humid argon/liquid sample in duplicates at 5 and 20 min). Graphed: mean  $\pm$  SEM.

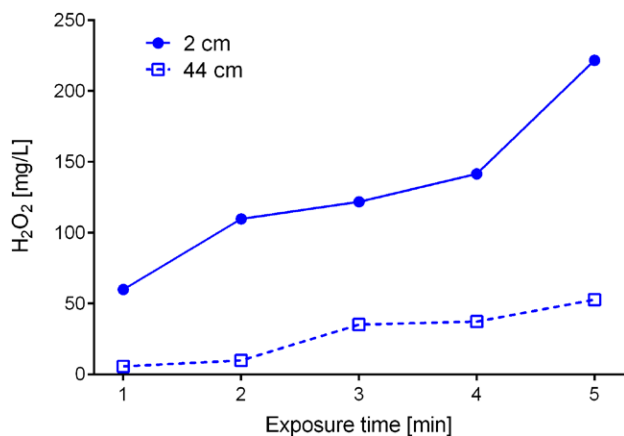


**Figure 12.** H<sub>2</sub>O<sub>2</sub> concentration at 2 (circle symbols) and 44 cm (square symbols) in water droplets ( $5 \times 10 \mu\text{L}$ ) over increasing exposure times to the plasma discharge in humid argon (760 ppm H<sub>2</sub>O). Experiments were carried out in triplicates.

#### 4.1. Temperature and desiccation

The plasma process is carried out at room temperature. The steady state temperatures measured on the quartz surface and in the gas flow at the outlet always remained within the permissive range for the bacterial species. In the case of *E. coli* used here as the model bacteria, the measured temperature of 30 °C will not induce a thermal shock response (temperature step with fast rise). In addition, this temperature is below the optimal temperature of growth for this bacterium. Based on the absence of significant bacterial viability loss in the control treatments, the desiccation effects of the gas flow are not significant bactericidal factors by themselves. Nevertheless, desiccation is enhanced during plasma operation: A hydration loss from phospholipids of the bilayer membrane induces membrane separation, leading to protein aggregation, and upon rehydration, membrane modifications lead to solute leakage and loss [43]. Moreover, fast desiccation can induce protein conformational changes, resulting in dysfunctions in enzymes and electron transport chains that cause free radical accumulation. This can influence the cell's capacity to alleviate the damages generated by the plasma and may result in lipid peroxidation, protein denaturation, and DNA mutation [37].

We also measured local and transient (duration  $\sim 2 \mu\text{s}$ ) high temperatures ( $450 \pm 50 \text{ K}$ ) at different positions along the path of the discharge propagation. This was done using spectroscopic measurements (figure 8) compared with modelling of the nitrogen second positive system. The effect of this transient thermal stress on bacteria is unknown. However, the same thermal stress (within the  $\pm 50 \text{ K}$  error range) was applied on the sample whatever its location inside the tube (2 cm and 44 cm), and yet, this thermal stress cannot account for the difference in decontamination efficiency observed between these two locations, so its contribution to the overall bactericidal effect can be neglected. It can be added that the surface discharges, during their propagation, may induce transient electric field changes on the cell membranes but this effect does not seem important from our results and was not further studied here.

#### 4.2. UV emission

Emissive argon species and hydroxyl radicals generate UV-A, and -B emissions that inflict further damage on cells. While DNA is the primary target for UV-induced damage [44, 45], other UV-absorbing cell components can be targeted as well, such as proteins. The high energy photons from the short-wavelength UV radiation can lead to singlet oxygen and free radical formation when absorbed by molecules of chromophores, and can generate molecular singlet oxygen  $\text{O}_2^1\Delta_g$  ( $^1\text{O}_2$ ) through type II photosensitization reactions that will target membranes and other cellular components [46, 47]. Furthermore, a single photon impact on the DNA molecule may have a lethal effect at the cellular level. Most damage to the DNA can be attributed to UV-B (280–315 nm) emission that is absorbed by cellular DNA. UV-A (315–400 nm), while less potent, may generate indirect damage to the DNA via photoreactions and photosensitization [48]. UV-induced DNA modifications are presented by pyrimidine dimers of thymine-thymine or thymine-cytosine [49]. These lesions will result in DNA helix distortion and block transcription and replication that can generate punctual mutations and lead to cell death [50, 51].

In figure 7, the relative UV-B dose (305–311 nm) per discharge event calculated for each sample position along the tube is presented. This relative dose can be extrapolated to calculate an accumulated relative UV-B dose for the two different positions at different treatment durations. This accumulated relative dose (now normalized to the 2 cm, 20 min case) is then used as the abscissa for figure 13. In figure 13(A), the reduction factor of bacteria samples deposited onto the external surface of the quartz tube (OUT samples: only submitted to the plasma UV-B emission) increases with the accumulated relative UV-B dose. The most important result extracted from data in figure 13(A) is that no major difference in the trend may be discerned between points at the two positions (open and closed symbols), which means that the bactericidal efficiency on the OUT samples only depends on the relative UV-B dose. From a qualitative point of view, the observed tendency is in agreement with *E. coli* (wild type and mutants) UV irradiation studies [52].

Another interesting point is that greater efficiency is observed for liquid samples as compared to dried ones (triangle symbols compared to circles). The influence of the sample form (dried or liquid) could be interpreted as due to a shadow effect previously invoked for the UV irradiation of multilayer microorganism samples [53] which occurs more in the dried samples. Another hypothesis to be verified in future is a possible chemical effect due to the H<sub>2</sub>O<sub>2</sub> in the water and its synergy with the direct UV-B effect.

In the case of a direct exposure of bacteria to the plasma (IN samples deposited inside the tube—figure 13(B), the reduction factor is no longer influenced by the form of the sample, but is strongly dependent on the sample location: for a given value of the accumulated relative UV-B dose (e.g. 0.25), the reduction factor at 2 cm is 3 log<sub>10</sub> higher than at 44 cm, either for dry and liquid samples. When focusing on bacteria exposed to plasma for the same duration, e.g. 20 min (open symbols at 0.25

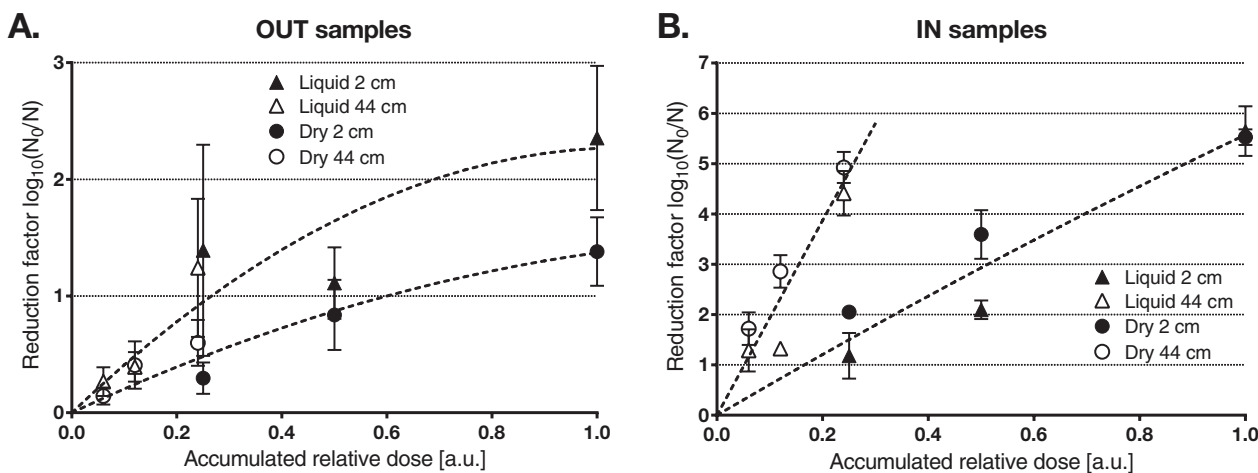


**Figure 13.** Reduction factor (data from figure 11) as a function of the calculated accumulated relative dose (with regard to samples positions in the tube and exposure time). Dashed lines are only guides for the eye. Graphed: mean  $\pm$  SEM.

relative dose and closed symbols at 1.0 relative dose), a similar reduction factor was obtained for 4-times higher dose received by the 2 cm sample (than the 44 cm sample). The bactericidal decontamination mechanism in the IN samples is therefore not governed by the UV-B irradiation dose and another stress factor dominates. It was observed that exposure of DNA to radiation from noble gas radiofrequency discharge did not lead to single strand nor double strand break [54]. Although, direct contact of DNA with a helium plasma needle (propagating in open air) induced single strand break [55], and exposure to humid argon post-discharge induced DNA fragmentation [16].

Another potential biocidal factor is VUV radiation (200–10 nm) from the second continuum of the argon excimer  $\text{Ar}_2^*$  (maximum intensity at 126 nm).  $\text{Ar}_2^*$  results from a three-body collision mechanism of two ground state Ar atoms with an excited  $\text{Ar}^*$  atom. This type of radiation has a low penetration depth in air, but in the case of an argon atmosphere the penetration depth is much longer because the excimer radiation is not subject to self-absorption [56]. The rare gas excimer emissions produce photons with energies that can break most chemical bonds and initiate chemical reactions [57]. The maximum intensity of the argon excimer emission at 126 nm corresponds to energy of 9.84 eV, which is sufficient to cause photodissociation of water (4.77 eV being the dissociation energy for O–H bond). The quenching of  $\text{Ar}^*$  by  $\text{H}_2\text{O}$  molecules, as seen by the reduction of the argon emission intensity (700–850 nm) in the presence of water (figure 4), should lead to a decrease in the excimer second continuum emission intensity. Therefore, the bactericidal effect of VUV emission should be greater in dry argon and might be relatively limited in our most efficient plasma treatment settings that involve humid argon feed gas. In the specific case of dry argon and dried samples, the VUV emission could be considered as important for the samples placed inside the tube, and may contribute to the rather high decontamination efficiency shown in figure 11(D).

This VUV emission could also decrease or be quenched because of gas impurities, especially oxygen and nitrogen species [14, 57]. VUV/UV emission by itself can cause damage even on spores, but its biocidal effectiveness varies markedly with wavelength and power densities [4].

Samples placed onto the outer surface of the tube cannot be submitted to the VUV emission because of the tube material (quartz). Results show that the higher the water vapor content, the higher the decontamination efficiency (figure 12(A)). During experiments with liquid samples placed outside of the quartz tube, there were liquid samples placed inside. Through evaporation the inner samples contributed to an increase in the water vapor concentration inside the tube; and thus to an increase (at least for a period of time) in the OH emission intensity (UV-B) received by the outer samples.

Results obtained for samples placed inside the tube show that the conditions providing the greatest bactericidal effect are the humid argon discharge on dried samples, considering samples located 44 cm from the HV electrode. The  $\text{H}_2\text{O}$  molecules at a constant concentration in the argon gas generate both UV radiation and reactive species (i.e. OH in ground and excited states) that directly affect the dried bacterial cells. In the case of liquid samples, there is a dilution of the reactive species and so a delay in the bactericidal effect compared to the dried samples.

#### 4.3. Reactive oxygen species

Plasma generated in humid gases is known to produce hydrogen peroxide [19], the most stable reactive species generated by this process. The production rate of  $\text{H}_2\text{O}_2$  is dependent upon the water content of the plasma environment (feed gas and samples) that determines the production of OH radicals, which are precursors of  $\text{H}_2\text{O}_2$ , and the degree of conversion of water into  $\text{H}_2$  and  $\text{O}_2$  [31]. Traces of hydrogen peroxide were accumulated in water after the plasma process. The impact of hydrogen peroxide on bacterial survival was examined. The incubation of bacterial cells in a solution of  $222 \text{ mg l}^{-1}$   $\text{H}_2\text{O}_2$  for a 5 min period, representing the same  $\text{H}_2\text{O}_2$  concentration as the one measured in the wet sample at 2 cm and 5 min plasma exposure (figure 13), resulted in a 0.1  $\log_{10}$  only reduction of bacterial viability, whereas a 5 min exposure time to the plasma (humid argon/liquid sample) led to a 1.2–1.3  $\log_{10}$  reduction (for both 2 cm and 44 cm positions). The similar reduction factors were here obtained with

very different hydrogen peroxide concentrations (222 mg l<sup>-1</sup> measured at 2 cm and 53 mg l<sup>-1</sup> measured at 44 cm). We can thus conclude that H<sub>2</sub>O<sub>2</sub> alone is not responsible for significant bacterial population reduction, although longer treatment times may affect the dryness of the sample and may interfere or amplify this effect in our current procedures. Nevertheless, higher hydrogen peroxide concentrations than those presented in figure 13 are expected since H<sub>2</sub>O<sub>2</sub> accumulates in liquid phase with time until the point when advanced evaporation takes place and when bacteria are only submitted to gas phase H<sub>2</sub>O<sub>2</sub> (low concentration). There should be an optimum exposure time corresponding to a maximum liquid phase H<sub>2</sub>O<sub>2</sub> concentration. Before full desiccation at this point bactericidal effect of hydrogen peroxide is not excluded, especially in combination with UV light.

Despite the low concentrations of formed H<sub>2</sub>O<sub>2</sub> were not shown to have an important decontamination effect, H<sub>2</sub>O<sub>2</sub> precursors, gas-phase OH radicals are known to be extremely reactive although very short-lived. They can be one of the major decontamination factors in the IN samples where the effect of UV-B was not found dominant.

As with the other stressors of argon plasma studied here, synergistic effects may occur allowing an efficient decontamination of bacterial cells even with stressors in limited concentrations. One of these may be the *in situ* production of OH radicals by UV photolysis of hydrogen peroxide [58].

## 5. Conclusion

This paper reports on biocidal results obtained with an atmospheric pressure non-thermal pulsed corona discharge plasma source adapted to the treatment of the inner surfaces of thin long tubes such as endoscope ducts or catheters. We report the full propagation of a streamer-like discharge inside a 2 mm diameter silicon tube over a distance of one meter. We investigated the bactericidal factors accounting for the decontamination effects, in particular the UV-B emission, in a quartz tube adapted to bacteria sample treatment and recovery and to optical emission diagnostics. To obtain a large enough mortality response to UV light only exposure, we chose to use a recA- *E. coli* strain.

The discharge feed gas was argon, (dry or with water vapor admixture). Although the treatment duration was longer than other non-thermal atmospheric pressure plasmas using air (which also produce harmful and stable species such as nitrogen oxides and ozone), the investigated plasma process allowed, using this *E. coli* strain, a ~5 log<sub>10</sub> reduction from a 10<sup>6</sup> initial population for samples placed 44 cm away from the HV electrode and for a 20 min exposure time.

Among the factors accounting for the observed bactericidal activity, it was determined that desiccation did not lead to strong population reduction (less than 1 log<sub>10</sub>). For the selected operating conditions, the temperature measured on the tube wall did not exceed 29 °C (at a 25 °C room temperature) and thus should not be an important stress factor either. On the other hand, short-duration (~2 μs) temperature increases were also measured in discharge channel during its propagation on

the inner surface of the tube (up to 450 ± 50 K). Given that (i) the temperature was found to be constant (within the error range) with distance, and (ii) the decontamination efficiency was, for a given exposure time, strongly dependent on the sample location, it was concluded that this transient heating did not play a major role in the decontamination.

By calculating the accumulated relative UV-B dose and comparing samples placed either inside or outside the quartz tube, it was determined that increased bacteria population reduction observed inside the tube may be due either to direct attack by reactive species such as OH or by synergistic effects such as UV hydrolysis of the formed hydrogen peroxide. The hydrogen peroxide production and its impact on bacterial survival were examined for short exposure duration. Bacteria incubation in a H<sub>2</sub>O<sub>2</sub> solution of the same and higher concentration as those measured in wet samples led to a negligible population reduction. It is thus concluded that hydrogen peroxide by itself is not responsible for significant bacterial reduction in these conditions. However, higher hydrogen peroxide concentrations are expected with longer treatment times, and therefore a bactericidal effect of hydrogen peroxide cannot be completely excluded.

OH production depends on water vapor content, and the latter can come from both liquid sample evaporation and/or addition of water vapor to the feed gas. This point was investigated, and from a practical point of view it was found that it is more effective to dry the surfaces prior to exposure to the plasma process and to add water vapor to the discharge feed gas.

## Acknowledgments

This work was supported by the Laboratories of Excellence LaSIPS from Campus Paris Saclay and by the French Foreign Office, and by Slovak Research and Development Agency APVV-0134-12.

## References

- [1] Bryers J 2008 *Biotechnol. Bioeng.* **100** 1–17
- [2] Kong M G, Groesen G, Morfill G, Nosenko T, Shimizu T, van Dijk J and Zimmermann J L 2009 *New J. Phys.* **11** 115012
- [3] Laroussi M 2002 *IEEE Trans. Plasma Sci.* **30** 1409
- [4] Lerouge S, Fozza A C, Wertheimer M R, Marchand R and Yahia L H 2000 *Plasmas Polym.* **5** 31–46
- [5] Moisan M, Barbeau J, Crevier M-C, Pelletier J, Philip N and Saoudi B 2002 *Pure Appl. Chem.* **74** 349–58
- [6] Villegier S, Cousty S, Ricard A and Sixou M 2003 *J. Phys. D: Appl. Phys.* **36** L60
- [7] Boudam M K, Saoudi B, Moisan M and Richard A 2007 *J. Phys. D: Appl. Phys.* **40** 1694
- [8] Fumagalli F, Kylian O, Amato L, Hanus J and Rossi F 2012 *J. Phys. D: Appl. Phys.* **45** 135203
- [9] Odic E, Goldman A, Goldman M, Delaveau S, Le Hégarat F 2002 *J. High Temp. Mater. Process.* **6** 385–96
- [10] Kirkpatrick M J, Dodet B and Odic E 2007 *Int. J. Plasma Environ. Sci. Technol.* **1** 96–101
- [11] Kamgang J O, Briandet R, Herry J M, Brisset J-L and Naïtali M 2007 *J. Appl. Microbiol.* **103** 621–8

- [12] Kamgang-Youbi G, Herry M-J, Meylheuc T, Brisset J-L, Bellon-Fontaine M-N, Doubla A and Naitali M 2009 *Lett. Appl. Microbiol.* **48** 13–8
- [13] Sarrette J-P, Cousty S, Merbahi N, Nègre-Salvayre A and Clément F 2010 *Eur. Phys. J. Appl. Phys.* **49** 13108
- [14] Polak M, Winter J, Schnabel U, Ehlbeck J and Weltmann K-D 2012 *Plasma Process. Polym.* **9** 67–76
- [15] Limam S, Odic E, Kirkpatrick M J and Pointu A-M 2013 *Plasma Process. Polym.* **10** 679–85
- [16] Odic E, Limam S, Kirkpatrick M J, Dodet B, Salamitou S and DuBow M S 2012 Investigations of bacterial inactivation and DNA fragmentation induced by flowing humid argon post-discharge *NATO ARW Plasma for Bio-Decontamination, Medicine and Food Security (NATO ASI Series)* ed Z Machala (Dordrecht: Springer) pp 93–106 Chapt. 8
- [17] Dodet B, Odic E, Salamitou S, Goldman A and Goldman M 2006 *Proc. of the 10th Int. Symp. on High Pres. Low Temp. Plasma Chemistry (HAKONE X)* (Saga, Japan) pp 355–8
- [18] Oehmigen K, Hähnel M, Brandenburg R, Wilke Ch, Weltmann K-D and von Woedtke Th 2010 *Process. Polym. Plasma Med.* **7** 250–7
- [19] Dodet B, Odic E, Goldman A, Goldman M and Renard D 2005 *J. Adv. Oxid. Technol.* **8** 91–7
- [20] Robert E, Barbosa E, Dozias S, Vandamme M, Cachoncinlle C, Viladrosa R and Pouvesle J M 2009 *Plasma Process. Polym.* **6** 795–802
- [21] Dang Van Sung, Mussard M, Guaitella O and Rousseau A 2013 *J. Phys. D: Appl. Phys.* **46** 302001
- [22] Park S, Choe W, Kim H and Park J Y 2015 *Plasma Sources Sci. Technol.* **24** 034003
- [23] Maletic D, Puac N, Selakovic N, Lazovic S, Malovic G, Dordevic A, Petrovic Z L J 2015 *Plasma Sources Sci. Technol.* **24** 025006
- [24] Lu X, Naidis G V, Laroussi M and Ostrikov K 2014 *Phys. Rep.* **540** 123–66
- [25] Lu X, Laroussi M and Puech V 2012 *Plasma Sources Sci. Technol.* **21** 034005
- [26] Lefebvre J and Ricard A 1975 *Rev. Phys. Appl.* **10** 137–42
- [27] Laux C O, Spence T G, Kruger C H and Zare R N 2003 *Plasma Sources Sci. Technol.* **12** 125–38
- [28] Hanahan D 1983 *J. Mol. Biol.* **166** 557–80
- [29] van Veldhuizen E M and Rutgers W R 2002 *J. Phys. D: Appl. Phys.* **35** 2169–79
- [30] Sobota A, Lebouvier A, Kramer N J, van Veldhuizen E M, Stoffels W W, Manders F and Haverlag M 2009 *J. Phys. D: Appl. Phys.* **42** 15211
- [31] Kozlov K V, Odic E, Tatarenko P A, Dodet B, Fedoseev G S, Kirkpatrick M J, Samoilovich V G and Ganciu M 2006 *Proc. of the 10th Int. Symp. On High Pressure, Low Temperature Plasma Chemistry (HAKONE X)* (Saga, Japan)
- [32] Hibert C, Gaurand I, Motret O, Pouvesle J M 1999 *J. Appl. Phys.* **85** 7070–5
- [33] Lu X and Laroussi M 2006 *J. Appl. Phys.* **100** 063302
- [34] Naidis G V 2010 *J. Phys. D: Appl. Phys.* **43** 402001
- [35] Winter J, Wende K, Masur K, Iseni S, Dünnbier M, Hammer M U, Tresp H, Weltmann K-D and Reuter S 2013 *J. Phys. D: Appl. Phys.* **46** 295401
- [36] Hensel K et al 2015 *Biointerphases* **10** 029515
- [37] Potts M 1994 *Microbiol. Rev.* **58** 755
- [38] Billi D and Potts M 2000 Life without water: responses of prokaryotes to desiccation *Environmental Stressors and Gene Responses* ed K B Storey and J M Storey (Amsterdam: Elsevier) 181–92
- [39] Arjunan K P, Sharma V K and Ptasincka S 2015 *Int. J. Mol. Sci.* **16** 2971–3016
- [40] Davies K J A 2000 *IUBMB Life* **50** 279–89
- [41] Rutala W A, Weber J D and The Healthcare Infection Control Practices Advisory Committee: Guideline for Disinfection and Sterilization in Healthcare Facilities 2008 *Centers for Disease Control and Prevention (CDC)* (Chapel Hill, NC: Department of Health and Human Services USA)
- [42] Finnegan M, Linley E, Denyer S P, McDonnell G, Simon C and Maillard J-Y 2010 *J. Antimicrob. Chemother.* **65** 2108–15
- [43] Crowe J H, Crowe L M, Carpenter J E, Petrelski S, Hoekstra F A, De Araujo P and Panel A D 1997 Anhydrobiosis: cellular adaptation to extreme dehydration *Handbook of physiology* ed W H Dantzer vol II (Oxford: Oxford University) pp 1445–78
- [44] Peak M J and Peak J G 1982 *Photochem. Photobiol.* **35** 675–80
- [45] Peak M J, Peak J G, Moehring P and Webb R B 1984 *Photochem. Photobiol.* **40** 613–20
- [46] Alschér R G, Donahue J L and Cramer C L 1997 *Physiol. Plant.* **100** 224–33
- [47] Mackerness S A H, Jordan B R and Thomas B 1999 *J. Photochem. Photobiol.* **48** 180–8
- [48] Sinha R P and Hader D P 2002 *Photochem. Photobiol. Sci.* **1** 225–36
- [49] Lindahl T and Wood R D 1999 *Science* **286** 1897–905
- [50] Britt A B 1995 *Plant. Physiol.* **108** 891–6
- [51] Lindahl T 1993 *Nature* **362** 709–15
- [52] Clauß M and Grotjohann N 2009 *Mutation Res.* **673** 83–6
- [53] Moisan M, Barbeau J, Moreau S, Pelletier J, Tabrizian M, Yahia L H 2001 *Int. J. Pharm.* **226** 1–21
- [54] O'Connell D, Cox L J, Hyland W B, McMahon S J, Reuter S, Graham W G, Gans T and Currell F J 2011 *Appl. Phys. Lett.* **98** 043701
- [55] Lazovic S, Maletic D, Leskovac A, Filipovic J, Puac N, Malovic G, Joksic G and Petrovic Z L J 2014 *Appl. Phys. Lett.* **105** 124101
- [56] Heise M, Neff W, Franken O, Muranyi P and Wunderlich J 2004 *Plasma Polym.* **9** 23–33
- [57] Masoud N, Martus K and Becker K 2005 *J. Phys. D: Appl. Phys.* **38** 1674–83
- [58] Crittenden J C, Hu S and Hand D W 1999 *Water Res.* **33** 2315–28